Stability of Imperfect Laminated Cylinders: A Comparison Between Theory and Experiment

George J. Simitses,* Dein Shaw,† and Izhak Sheinman‡
Georgia Institute of Technology, Atlanta, Georgia

A comparison between analytical results (critical loads) and experimental results (buckling loads) is presented for imperfect, laminated, circular, cylindrical, thin shells. The loading consists of uniform axial compression and torsion, applied individually and in combination (load cases for which results are published in the open literature). The imperfection shape and amplitude of the experimental results are explicitly given for some data and not for others. In the latter case, the comparison is qualitative. The theoretical results are obtained from a solution methodology that was developed and previously reported by the authors. It is based on nonlinear kinematic relations, linearly elastic material behavior, and the usual lamination theory. The comparison serves as an experimental verification for the analytical solution scheme.

I. Introduction

THE thin, circular, cylindrical shell has been used extensively as a structural configuration, especially in the aerospace industry. Because of this, this system has received tremendous attention with respect to specific questions of behavior when subjected to external loads. In particular, several reported investigations have dealt with the degree of approximation involved in the use of various kinematic relations (which led to several linear and nonlinear shell theories), others with the discrepancy between "linear theory" and experimental results for the buckling of shells (which led to postbuckling analyses and imperfection sensitivity studies), and still others with the use of external stiffening and with the effect of support conditions, cutouts, etc. These studies have led to a better understanding of shell behavior, but they have considered primarily shells of metallic construction.

In recent years, the increasing need for lightweight efficient structures has led the structural engineer to the field of structural optimization and simultaneously to the use of nonconventional materials such as fiber-reinforced composites. Such composites are attractive because of their high stiffness- and/or strength-to-weight ratios.

Much work has been done in the area of material properties characterization, analysis, fabrication, and design of composite structures. Tennyson[1] reviewed previous stability analyses of laminated cylinders. Since the several studies have reported comparisons of various shell theories for estimating critical loads (using linear buckling analyses), others have dealt with the effect of eccentric stiffening, and some with the effect of initial geometric imperfections (for a detailed discussion, see Ref. 2).

In Ref. 2, the present authors discuss a solution methodology developed to analyze the response to imperfect, laminated, thin, circular, cylindrical shells subjected to destabilizing loads that are applied individually or in combination. The response includes prelimit point behavior, the establishment of limit points (critical conditions), as well as postlimit point behavior. The ends of the cylindrical shell can be supported in a general manner (simply supported, clamped, numerous combinations of in-plane boundary conditions, etc.) and the loads are either applied quasistatically (static buckling) or suddenly (dynamic buckling). The methodology is demonstrated by studying the response of several laminate configurations (symmetric, antisymmetric, and asymmetric) to static and sudden application of uniform axial compression.

However, the best means for establishing confidence in an analytical method is to compare it with experimental results obtained by researchers not connected with those who developed the analytical procedure.

The purpose of the present paper is to present such a comparison. The literature was searched and two sets of experimental results were found: 1) those for which the imperfect geometry is described in terms of imperfection shape and amplitude and 2) those for which there are no data describing the initial geometric imperfection. Moreover, the load cases considered are uniform axial compression and torsion, applied either individually or in combination.

The comparison for class 1 is direct, because both the shape and amplitude of the initial geometric imperfection are known. On the other hand, for class 2 geometries, the comparison is made by assuming a shape for the initial geometric imperfection and by varying the amplitude from some small fraction of the total thickness (5-10%) to over 50% of the total thickness. Clearly, the comparison is more of qualitative nature for this class of imperfect geometries.

Before discussing the geometries employed in the experiments, their theoretical analyses, and the comparison between critical (theoretical) and buckling (experimental) loads, a brief description of the governing equations and the solution scheme are presented.

II. Governing Equations

The details of the mathematical formulation can be found in Ref. 2. The governing equations are derived for an orthogonally stiffened laminate, subjected to eccentric in-plane loads and uniform external pressure. The nonlinear governing equations (equilibrium) and related boundary conditions are derived from the principle of the stationary value of the total potential and they are based on Donnell-type nonlinear kinematic relations and linearly elastic material behavior. Moreover, the smeared technique is used for the orthogonal stiffeners.[2] Introduction of an Airy stress (resultant) func-

Presented as Paper 83-0874 at the AIAA/ASME/ASCE/AHS 24th Structures, Structural Dynamics and Materials Conference, Lake Tahoe, Nev., May 2-4, 1983; received June 28, 1983; revision submitted July 29, 1984.

*Professor, Engineering Science and Mechanics. Associate Fellow AIAA.

†Research Associate, Engineering Science and Mechanics.

‡Visiting Scholar (presently Senior Lecturer, Civil Engineering, Technion—Israel Institute of Technology, Haifa, Israel).

tion F defined as

$$N_{xx} = -\bar{N}_{xx} + F_{,yy}; \quad N_{yy} = F_{,xx}; \quad N_{xy} = \bar{N}_{xy} - F_{,xy} \tag{1}$$

leads to the identical satisfaction of the two in-plane equilibrium equations, where N_{xx} and N_{xy} are the applied in-plane loads. With this, the field equations are the third (transverse) equilibrium equation and the (in-plane) compatibility equation. Both of these, as well as the related boundary conditions, are expressed solely in terms of w and F and their space-dependent derivatives. These are

1) Equilibrium:

$$\begin{aligned} &b_{11}F_{,yyxx} + b_{21}F_{,xxxx} - b_{31}F_{,xxxy} + d_{11}w_{,xxxx} + d_{12}w_{,xxyy} \\ &+ 2d_{13}w_{,xxxy} + 2b_{13}F_{,xyyy} + 2b_{23}F_{,xxxy} - 2b_{33}F_{,xxyy} \\ &+ 2d_{31}w_{,xxxy} + 2d_{32}w_{,xyyy} + 4d_{33}w_{,xxyy} + b_{12}F_{,yyyy} \\ &+ b_{22}F_{,xxyy} - b_{32}F_{,xyyy} + d_{21}w_{,xxyy} + d_{22}w_{,yyyy} + 2d_{23}w_{,xyyy} \\ &- F_{,xx} + F_{xx}(w_{,xx} + w^{\circ}_{,xx}) - \bar{N}_{xx}(w_{,xx} + w^{\circ}_{,xx}) \\ &+ 2\bar{N}_{xy}(w_{,xy} + w^{\circ}_{,xy}) - 2F_{,xy}(w_{,xy} + w^{\circ}_{,xy}) \\ &+ F_{,xx}(w_{,yy} + w^{\circ}_{,yy}) + q = 0 \end{aligned} \tag{2}$$

2) Compatibility

$$\begin{aligned} &a_{11}F_{,yyyy} + a_{12}F_{,xxyy} - a_{13}F_{,xyyy} + b_{11}w_{,xxyy} + b_{12}w_{,yyyy} \\ &+ 2b_{13}w_{,xyyy} + a_{12}F_{,xxyy} + a_{22}F_{,xxxx} - a_{23}F_{,xxxy} + b_{21}w_{,xxxx} \\ &+ b_{22}w_{,xxyy} + 2b_{23}w_{,xxxy} - a_{13}F_{,xyyy} - a_{23}F_{,xxxy} + a_{33}F_{,xxyy} \\ &- b_{31}w_{,xxxy} - b_{32}w_{,xyyy} - 2b_{33}w_{,xxyy} = -(w_{,xx}/R) \\ &+ w_{,xy}(w_{,xy} + 2w^{\circ}_{,xy}) - \tfrac{1}{2}w_{,xx}(w_{,yy} + 2w^{\circ}_{,yy}) \\ &- \tfrac{1}{2}w_{,yy}(w_{,xx} + 2w^{\circ}_{,xx}) \end{aligned} \tag{3}$$

where a_{ij}, b_{ij}, and d_{ij} are the elements of the matrices that relate the reference surface strains ϵ°_{ij} and moment resultants M_{ij} to the stress resultants N_{ij} and the reference surface changes in curvature and torsion (for details, see Ref. 2). In matrix form, these relations are

$$\{\epsilon^{\circ}_{ij}\} = [a_{ij}]\{N_{ij}\} + [b_{ij}]\{\kappa_{ij}\} \tag{4}$$

$$\{M_{ij}\} = [b_{ij}]^T\{N_{ij}\} + [d_{ij}]\{\kappa_{ij}\} \tag{5}$$

where

$$[a_{ij}] = [\bar{A}_{ij}]^{-1}; \quad [b_{ij}] = [\bar{A}_{ij}]^{-1}[\bar{B}_{ij}] \tag{6}$$

and

$$[d_{ij}] = [\bar{B}_{ij}][b_{ij}] - [\bar{D}_{ij}] \tag{7}$$

Note that $[\bar{A}_{ij}]$, $[\bar{B}_{ij}]$, and $[\bar{D}_{ij}]$ are the matrices obtained from the usual lamination theory[3] and smeared technique for the stiffeners[4] when relating stress and moment resultants to reference surface strains and changes in curvature and torsion.

Moreover, the boundary conditions (at $x=0,L$) for cases of simple and clamped supports and all possible combinations of in-plane conditions can be written, using the notation of Ref. 5, as

$$\begin{aligned} &\text{SS-1:} \quad w=0;\ M_{xx}=\bar{M}_{xx};\ N_{xx}=-\bar{N}_{xx};\ N_{xy}=\bar{N}_{xy} \\ &\text{SS-2:} \quad w=0;\ M_{xx}=\bar{M}_{xx};\ u=\text{const};\ N_{xy}=\bar{N}_{xy} \\ &\text{SS-3:} \quad w=0;\ M_{xx}=\bar{M}_{xx};\ N_{xx}=-\bar{N}_{xx};\ v=\text{const} \\ &\text{SS-4:} \quad w=0;\ M_{xx}=\bar{M}_{xx};\ u=\text{const};\ v=\text{const} \end{aligned} \tag{8}$$

and

$$\begin{aligned} &\text{CC-1:} \quad w=0;\ w_{,x}=0;\ N_{xx}=-\bar{N}_{xx};\ N_{xy}=\bar{N}_{xy} \\ &\text{CC-2:} \quad w=0;\ w_{,x}=0;\ u=\text{const};\ N_{xy}=\bar{N}_{xy} \\ &\text{CC-3:} \quad w=0;\ w_{,x}=0;\ N_{xx}=-\bar{N}_{xx};\ v=\text{const} \\ &\text{CC-4:} \quad w=0;\ w_{,x}=0;\ u=\text{const};\ v=\text{const} \end{aligned} \tag{9}$$

where $\bar{M}_{xx} = -\bar{E}\bar{N}_{xx}$, and $\bar{E}$ represents the eccentricity (distance from the reference surface) of the applied stress resultant $\bar{N}_{xx}$, the eccentricity is positive if in the positive z direction. The above boundary conditions may be written in terms of the dependent variables F and w.

III. Analytical Solution Scheme

The solution methodology is described in detail in Ref. 2. A brief description is presented below. The solution scheme consists of the following steps:

1) A separated form for the dependent variables is first introduced. This is given by

$$\begin{aligned} w(x,y) &= A_0(x) + \sum_{i=1}^{k}\left[A_i(x)\cos\frac{iny}{R} + B_i(x)\sin\frac{iny}{R}\right] \\ F(x,y) &= C_0(x) + \sum_{i=1}^{2k}\left[C_i(x)\cos\frac{iny}{R} + D_i(x)\sin\frac{iny}{R}\right] \end{aligned} \tag{10}$$

In addition, the initial geometric imperfection $w^{\circ}(x,y)$ is presented in a similar form

$$w^{\circ}(x,y) = A^{\circ}_0(x) + \sum_{i=1}^{k}\left[A^{\circ}_i(x)\cos\frac{iny}{R} + B^{\circ}_i(x)\sin\frac{iny}{R}\right] \tag{11}$$

2) The expressions for w, F, and w° [Eqs. (10) and (11)] are substituted into the in-plane compatibility equation. Through trigonometric identities involving the products, the equation is written in a complete Fourier series form, from $i=0$ to $2k$. Use of orthogonality yields $(4k+1)$ nonlinear, ordinary, differential equations in the $(6k+2)$ Fourier coefficients [A_0, A_i, B_i, C_0, C_i, and D_i, see Eqs. (10)].

3) The Galerkin procedure is employed in connection with the transverse equilibrium equation (in the circumferential direction only). This leads to the vanishing of $(2k+1)$ Galerkin integrals, which yields $(2k+1)$ nonlinear, ordinary, differential equations in the same unknowns. Note that the number of equations and unknowns is $(6k+2)$.

4) Moreover, the associated boundary conditions, the expression for the total potential, and the expressions for the average end shortening and average in-plane shear strain are also presented in terms of the unknown functions (A, B, C, and D).

5) The nonlinear system of differential equations is then reduced to a sequence of linearized (with small changes in the dependent variables) equations by employing a generalization of Newton's method[6] applicable to differential equations. The linearized iteration equations are derived based on the premise that a solution can be achieved by a small correction to an approximate solution.

6) Finally, the linearized set of differential equations is cast into a system of finite difference equations by employing the usual central difference formula. These equations are then solved by an algorithm that is a modification of one described in Ref. 7. For details, see Ref. 8.

For finding prelimit point equilibrium positions, the applied load parameter is taken as known. For small values of the applied load, the linear solution is taken to be the approximate solution and the small corrections are obtained through the solution of the linearized iteration equations. Note that the stiffness matrix is positive definite in this range.

For finding postlimit point equilibrium positions (in a range of a possibly negative stiffness matrix), the numerical scheme is modified. The load parameter is taken to be unknown and one of the displacement Fourier coefficients, A_i and B_i, replaces it as a known parameter. In this range, the last converged prelimit point solution is used as an initial estimate (needed for an approximate solution) for the linearized iteration equations (see Ref. 8 for the solution algorithm). Once a postlimit point solution (equilibrium point) is established, the previous solution is utilized as an initial estimate for the iteration equations.

Finally, numerical integration is used to find the values of the total potential, end shortening, and average in-plane shear strain. By this procedure, the entire load displacement, load end shortening, or load-averaged shear strain curve can be obtained for a given imperfection and each wavenumber n. At each load level the n value that minimizes the total potential is taken as corresponding to the correct response.

IV. Description of Geometries

The experimental results used here for comparison with the theoretical predictions are obtained from four sources. The first is an unpublished paper presented by Kobayashi et al. in 1982.[9] The presentation took place in a "Work-in-Progress" session on structures. At the time, the author supplied an addendum to his abstract that described the experimental results on graphite-epoxy composite cylinders in axial compression. Through this information and private communication that followed, the complete description was secured and is listed herein as group A. The imperfection amplitude and shape are not known for this group.

The second source is a 1976 University of Toronto report[10] in which analytical and experimental results are given for imperfect glass/epoxy cylinders subjected to combined loading. Only one set of results is employed herein and it is listed as group B. Information concerning the imperfection shape and amplitude is provided by the author and listed below. The load case for this group is a combined application of axial compression and torsion.

The third source is a 1974 paper[11] that presents experimental results for boron/epoxy and graphite/epoxy imperfect cylinders subjected to axial compression and torsion, applied either individually or in combination. Certain geometries from this reference are employed herein. These configurations are listed below as group C. Information is not provided for the imperfection shapes and amplitudes.

Finally, the last source is a 1973 paper[12] that describes experimental and theoretical results on axially loaded glass/epoxy imperfect cylinders. This work was also performed at the University of Toronto under the direction of Prof. Tennyson. Three geometries from this source are employed herein and constitute group D. The imperfection shape and amplitude are supplied by Ref. 12.

In describing each group, information concerning the following is provided: load case, number of plies, stacking description and order, material and material properties, ply and laminate thickness, length and radius of the laminate, boundary conditions, and geometric imperfection. Each configuration in a group (if more than one) is listed as case Li, where i is an integer and L assumes the letters A, B, C, and D (group).

Group A (Kobayashi et al.[9])

1) Load: uniform axial compression
2) Material: graphite/epoxy
3) Material properties:

$$E_{11} = 17.40 \times 10^6 \text{ psi}; \quad E_{22} = 1.115 \times 10^6 \text{ psi}$$

$$G_{12} = 0.707 \times 10^6 \text{ psi}; \quad \nu_{12} = 0.32$$

4) Diameter and length: $2R = 7.874$ in., $L = 7.874$ in.
5) Boundary conditions: CC-4 ($u = \bar{u}$; $v = w = w_{,x} = 0$)
6) Imperfection: no information

So far, the data are common for all cases. Configurations are as follows.

Case A1:

Three-ply laminate (90/−20/20 deg)

$t_{\text{ply}} = 0.0055$ in., $t_{\text{tot}} = 0.0165$ in.

Case A2:

Four-ply laminate (90/−45/−45/0 deg)

$t_{\text{ply}} = 0.0057$ in., $t_{\text{tot}} = 0.0228$ in.

Case A3:

Six-ply laminate (90/90/30/−30/−30/30 deg)

$t_{\text{ply}} = 0.0059$ in., $t_{\text{tot}} = 0.0354$ in.

Note that all three configurations are asymmetric with respect to the midsurface. The stacking order starts from the outside of the cylinder and moves inward. Thus, in case A1, the outer ply strong axis (of orthotropy) makes a 90 deg angle with the longitudinal axis of the cylinder, the next ply makes a −20 deg angle, and the inner a 20 deg angle with the longitudinal axis.

Case A4: All data are the same as cases A1-A3 except as follows.

For this case,

$$E_{11} = 16.78 \times 10^6 \text{ psi}; \quad E_{22} = 0.922 \times 10^6 \text{ psi}$$

$$G_{12} = 0.707 \times 10^6 \text{ psi}; \quad \nu_{12} = 0.32$$

$t_{\text{ply}} = 0.00667$ in., $t_{\text{tot}} = 0.04$ in.

Six-ply laminate (0/60/60/−60/60/0 deg).

Note that, unlike the other three configurations in this group, this laminate is symmetric with respect to the midsurface.

Group B (Booton[10])

1) Load: combined axial compression and torsion
2) Material: glass/epoxy
3) Material properties:

$$E_{11} = 6.32 \times 10^6 \text{ psi}; \quad E_{22} = 1.74 \times 10^6 \text{ psi}$$

$$G_{12} = 0.78 \times 10^6 \text{ psi}; \quad \nu_{12} = 0.435$$

4) Diameter and length: $2R = 13.2$ in., $L = 12.4$ in.
5) Boundary conditions: CC-4 ($u = \bar{u}$; $v = w = w_{,x} = 0$).
6) Imperfection: $w^\circ(x,y) = (0.028)(0.027)\cos(17\pi x/L)$

where w° is positive inward; axisymmetric imperfection.

Only one configuration is used for this group.

Case B1:

Three-ply laminate (45/0/−45 deg)

$t_{ply} = 0.009$ in., $t_{tot} = 0.027$ in.

Group C (Wilkins and Love[11])

1) Load: combined axial compression and torsion
2) Material: boron/epoxy and graphite/epoxy
3) Material properties:

Boron/epoxy	Graphite/epoxy
$E_{11} = 30.0 \times 10^6$ psi	$E_{11} = 2.17 \times 10^6$ psi
$E_{22} = 2.7 \times 10^6$ psi	$E_{22} = 1.44 \times 10^6$ psi
$G_{12} = 0.65 \times 10^6$ psi	$G_{12} = 0.65 \times 10^6$ psi
$\nu_{12} = 0.21$	$\nu_{12} = 0.28$

4) Diameter and length: $2R = 15$ in., $L = 15$ in.
5) Boundary conditions: SS-3 ($N_{xx} = -N_{xx}$; $v = w = M_{xx} = 0$)
6) Imperfection: no information

These data are common for all cases. Configurations are as follows.

Case C1:

Four-ply boron/epoxy laminate (45/−45/−45/45 deg)

$t_{ply} = 0.053$ in., $t_{tot} = 0.0212$ in.

Case C2:

Six-ply graphite/epoxy laminate (0/45/−45/−45/45/0 deg)

$t_{ply} = 0.0056$ in., $t_{tot} = 0.0336$ in.

Note that both configurations are symmetric about the laminate midsurface. As in group A, the stacking sequence starts from the outside and moves inward.

Group D (Tennyson and Muggeridge[12])

1) Load: uniform axial compression
2) Material: glass/epoxy "Scotchply" (XP250)
3) Material properties: see below
4) Diameter and length: $2R = 12.5$ in., $L = 12.45$ in.
5) Boundary conditions: CC-4 ($u = \bar{u}$; $v = w = w_{,x} = 0$)
6) Imperfection: $w^\circ(x,y) = \xi t_{tot} \cos(m\pi x/L)$

Note that the laminate thickness t_{tot}, wavenumber m, and imperfection amplitude ξ depend on the configuration (case). Furthermore, the imperfection shape for all configurations, is axisymmetric.

The above data are common to all cases. Differences are as follows.

Case D1 (case 1a of Ref. 12):

Three-ply glass/epoxy laminate (0/70/−70 deg)

$E_{11} = 5.03 \times 10^6$ psi; $E_{22} = 2.58 \times 10^6$ psi

$G_{12} = 0.837$ psi; $\nu_{12} = 0.345$

$t_1 = t_2 = t_3 = 0.0009$ in. (t_i = thickness of each ply, from outer to inner: 1,2,3,)

$t_{tot} = 0.027$ in., $\xi = 0.0468$ ($\xi = w^\circ_{max}/t_{tot}$)

$m = 18$ (see the imperfection expression)

Case D2 (case 4a of Ref. 12):

Three-ply glass/epoxy laminate (45/−45/90 deg)

$E_{11} = 6.109 \times 10^6$ psi; $E_{22} = 2.69 \times 10^6$ psi

$G_{12} = 0.517 \times 10^6$ psi; $\nu_{12} = 0.317$

$t_1 = 0.009$ in.; $t_2 = t_3 = 0.0092$ in.

$t_{tot} = 0.0274$ in.; $\xi = 0.034$; $m = 18$

Case D3 (case 11a of Ref. 12):

Three-ply glass/epoxy laminate (30/90/30 deg)

$E_{11} = 5.42 \times 10^6$ psi; $E_{22} = 2.6 \times 10^6$ psi

$G_{12} = 0.687 \times 10^6$ psi; $\nu_{12} = 0.365$

$t_1 = t_3 = 0.009$ in.; $t_2 = 0.0093$ in.; $t_{tot} = 0.0273$ in.

$\xi = 0.0304$; $m = 17$

Note that all three configurations are asymmetric. Moreover, all data are taken from Ref. 12, in which the imperfection (axisymmetric) is given in the form of

$$w^\circ(x) = \xi t_{tot} \cos(qx/R) \tag{12}$$

The number q is given in Ref. 12. The imperfection expression is changed herein to be compatible with Eq. (11).

The solution methodology described in Ref. 2 is employed to compute critical (limit point) loads, which are then compared to the experimental results. This is easily done with the configurations for which the imperfection shape and amplitude are fully described. For the geometries for which no information about the imperfection is given, the comparison is more qualitative.

V. Theoretical Results and Discussion

The theoretical predicitons, based on the solution scheme of Ref. 2, and the comparison with the experimental results are discussed separately for each group of configurations.

Group A

Since no information is provided for this group, concerning the amplitude and shape of imperfection, the comparison is expected to be qualitative. It is assumed that the shape of imperfection is almost axisymmetric and the amplitude of imperfection is varied from a small fraction of the thickness to almost one thickness of the laminate,

$$w^\circ(x,y) = \xi t \left(\cos \frac{2\pi x}{L} + 0.1 \sin \frac{\pi x}{L} \cos \frac{ny}{R} \right) \tag{13}$$

Note that $|w^\circ_{max}| = 1.1\xi t$, where t is the laminate thickness.

Both the theoretical and the experimental results are shown in Table 1. The buckling load and the observed circumferential wavenumber are listed on columns two and three (data from Ref. 9). The next three columns list the theoretical results for three values of the imperfection amplitude parameter ξ. For case A1, the comparison suggests that the maximum imperfection amplitude for the tested geometry might be larger than one laminate thickness. Note that when $\xi = 1$ ($w^\circ_{max}/t = 1.1$), the theoretical load is 133.83 lb/in. For case A2, the comparison suggests that the "tested geometry" maximum imperfection amplitude is (approximately) $0.9t_{tot}$. Finally, the comparison for the other two cases (A3 and A4) is much better, since it suggests that the maximum imperfection amplitude is $0.4t_{tot}$.

Table 1 Theoretical and experimental results for group A

Geometry case	Experimental $\bar{N}^{\ell}_{xx}$, lb/in.	n	Theoretical $\bar{N}^{\ell}_{xx}$, lb/in.	n	ξ
A1	120.56	10	151.19	12	0.3
			140.55	12	0.5
			133.83	12	1.0
A2	248.46	8	362.30	9	0.1
			294.54	9	0.5
			231.83	9	1.0
A3	802.99	—	945.78	9	0.1
			872.99	9	0.3
			792.91	9	0.5
A4	892.02	—	944.66	10	0.2
			895.38	10	0.3
			798.51	10	0.5

Again, it is stressed that for this group the comparison is rather qualitative.

Group B

Only one geometry is taken from Ref. 10. According to this reference, the imperfection is axisymmetric and the experimental results are reported for a combined application of uniform axial compression and torsion. Theoretical predictions reported in Ref. 10 were obtained by employing a solution scheme that assumes axisymmetric prebuckling behavior and by finding those bifurcation loads corresponding to asymmetric behavior.

The present results, along with the theoretical predictions of Ref. 10 and the experimental findings, are presented graphically on Fig. 1. It can be seen that the agreement is very good for both positive and negative torques.

Group C

There is no information concerning the amplitude and shape of imperfection for this group. Thus, it is important to employ some shape for the imperfections and to vary the imperfection amplitude in order to approximate comparisons (qualitative) with the experimental results.[11]

Because the loading consists of both axial compression and torsion, three imperfection shapes are employed. The first is a virtually axisymmetric imperfection characterized by Eq. (13). The other two shapes correspond to approximations of the linear theory buckling modes for positive and negative torsion.[13]

In particular, Ref. 13 deals with solutions to the linearized buckling equations for the case of pure torsion. The Galerkin procedure is employed and the following approximate form for the buckling mode w^l used:

$$w^l(x,y) = \sum_{n=1}^{N}\sum_{m=1}^{M}\left(A_{mn}\cos\frac{ny}{R}+B_{mn}\sin\frac{ny}{R}\right) \times\left[\frac{L}{m\pi}\sin\frac{m\pi x}{L}-\frac{L}{(m+2)\pi}\sin\frac{(m+2)\pi x}{L}\right] \tag{14}$$

Because of orthogonality, only one n value is needed. A 10-term approximation ($m=5$) is obtained in Ref. 13. By studying the results, it is observed that the linear theory buckling mode is well approximated by two terms. This is accomplished by normalizing all coefficients in the 10-term approximation with respect to B_{2n}. A comparison of the order of magnitude of these coefficients shows that all but two are negligibly small. Finally, these two remaining coefficients are adjusted such that the maximum amplitude is ξt. Thus, one two-term approximation is used for positive torsion $w^\circ(+)$ and one two-term approximation for negative torsion $w^\circ(-)$. These expressions are applicable to both cases C1 and C2:

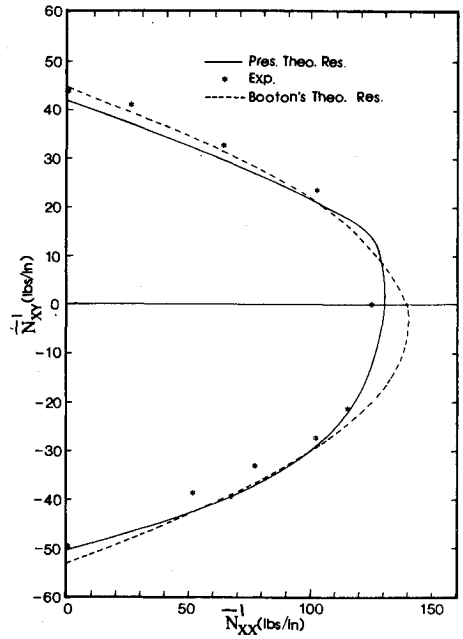

Fig. 1 Critical loads and buckling loads for group B.

$$w^\circ(+) = \xi t\left[0.05368\cos\frac{ny}{R}\left(\sin\frac{\pi x}{L}-\frac{1}{3}\sin\frac{3\pi x}{L}\right) -0.6710\sin\frac{ny}{R}\left(\sin\frac{2\pi x}{L}-\frac{1}{2}\sin\frac{4\pi x}{L}\right)\right] \tag{15}$$

$$w^\circ(-) = \xi t\left[0.5831\cos\frac{ny}{R}\left(\sin\frac{\pi x}{L}-\frac{1}{3}\sin\frac{3\pi x}{L}\right) +0.6479\sin\frac{ny}{R}\left(\sin\frac{2\pi x}{L}-\frac{1}{2}\sin\frac{4\pi x}{L}\right)\right] \tag{16}$$

Note that, for both Eqs. (15) and (16), by design

$$w^\circ_{\max}/t_{\text{tot}} = \xi \tag{17}$$

The generated results for each configuration are presented (in part) in both graphical and tabular form below.

Case C1

For the case of pure torsion, theoretical predictions are generated for the two imperfection shapes [Eqs. (15) and (16)] and for the positive and negative torsion of each shape. These theoretical predictions are shown as plots of the value of the critical (limit point) torsion $|\bar{N}^{\ell}_{xy}|$ vs the imperfection amplitude parameter ξ in Fig. 2. Note that, as the imperfection amplitude approaches zero, the results corresponding to the two shapes $w^\circ(+)$ and $w^\circ(-)$ approach the same value—as they should. Moreover, it is seen that the shape corresponding to Eq. (15) has a stabilizing effect at small values of ξ and for negative torsion.

The experimental value for positive and negative torsion are also noted in Fig. 2. For positive torsion, the experimental value is 26.5 lb/in. and the comparison with the theoretical result suggests that the imperfection amplitude is a little larger than one laminate thickness. On the other hand, for negative torsion, the experimental value is 65.7 lb/in. and the comparison suggests that the imperfection amplitude is less than two-tenths of the laminate thickness.

In addition, Ref. 11 provides experimentally obtained buckling interaction curves ($\bar{N}_{xx}$ vs $\bar{N}_{xy}$) for this geometry. Again, since the imperfection is not known, theoretical interaction curves are obtained analytically for two shapes of imperfection [Eqs. (13) and (15)] and various values for the imperfection amplitude parameter ξ. This comparison is for positive torsion and the results are shown graphically on Figs. 3 and 4. The experimental data are shown by the dashed line.

For this case, the comparison must be viewed as qualitative rather than quantitative.

Case C2

For this six-ply symmetric laminate, a qualitative type of comparison is presented only for positive torsion. The results are, in part, presented in Fig. 5 and Table 2.

Table 2 shows theoretical results obtained by the present analysis for two imperfection amplitude parameter values ($\xi = 0.05$ and 0.50) and the shape characterized by Eq. (15). First, the critical value corresponding to individual application of the loads are obtained and then the interaction curve is completed by assigning values for the applied torsion and finding the corresponding critical (limit point) axial compression. Note that the assigned values for the torsion are smaller than the individually applied critical torsion.

In Fig. 5, the experimental results of Ref. 11 and the theoretical prediction corresponding only to $\xi = 0.05$ are shown. The two curves seem to be very close for the entire range of interest. Thus, the comparison between experimental and theoretical interaction curves seems to be reasonable for this geometry.

Group D

There are several tests reported in Ref. 12. In all of these tests, the imperfection is axisymmetric. Theoretical critical loads are reported in Ref. 12, which were obtained by employing a linearized bifurcation analysis. The present

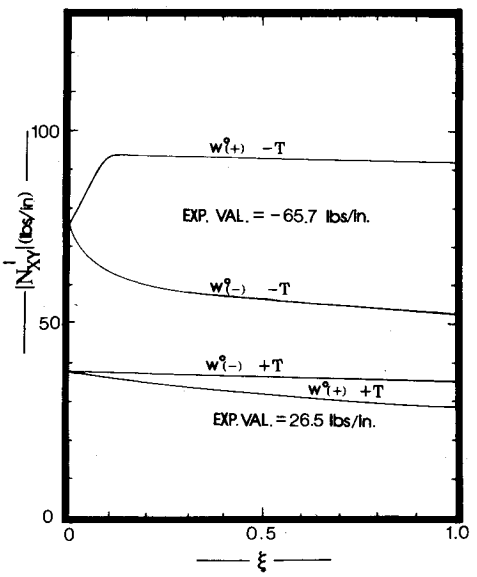

Fig. 2 $|\bar{N}^{\ell}_{xy}|$ vs the imperfection parameter ξ corresponding to two imperfection shapes, $w^{\circ}(+)$ and $w^{\circ}(-)$.

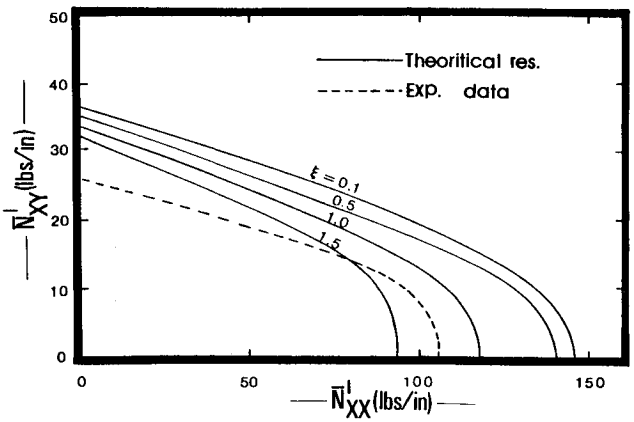

Fig. 3 Critical interaction curves [geometry C1, axisymmetric imperfection, Eq. (13)].

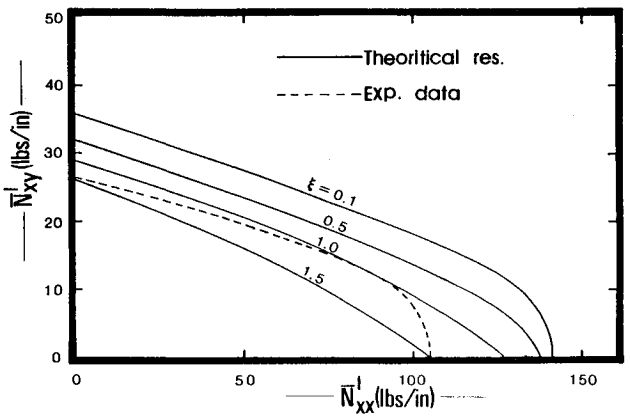

Fig. 4 Critical interaction curves [geometry C1, imperfection $w^{\circ}(+)$, Eq. (15)].

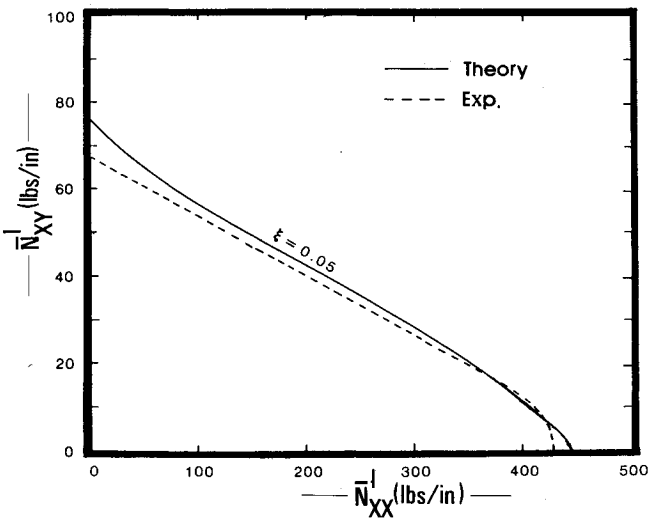

Fig. 5 Critical interaction curves [geometry C2, imperfection $w^{\circ}(+)$, Eq. (15)].

Table 2 Critical conditions for case C2

$\xi = 0.05$	$\bar{N}^{\ell}_{xx}$, lb/in.	442.6	348.1	232.3	70.32	0
	$\bar{N}^{\ell}_{xy}$, lb/in.	0	20	40	60	76.4
	n	13	13	12	13	12
$\xi = 0.50$	$\bar{N}^{\ell}_{xx}$, lb/in.	328.3	262.5	70.5	0	—
	$\bar{N}^{\ell}_{xy}$, lb/in.	0	15	14	61.4	—
	n	12	14	12	12	

Table 3 A comparison between theory and experiment for group D

Geometry case	Description of geometry					Ref. 12 results			Present results	
							$\bar{N}_{xx}$, lb/in.		$\bar{N}^{\ell}_{xx}$,	
	L, in.	t, in.	R/t	m	ξ	Test No.	Exp.	Theory	lb/in.	n
D1	12.42	0.0270	232	18	0.0468	1a	148.9	153.2	151.2	11
D2	12.45	0.276	267	18	0.0340	4a	142.0	165.1	174.5	11
D3	12.43	0.0273	229	17	0.0304	11a	149.1	185.2	174.3	11

methodology is employed and a comparison is made through Table 3.

For the first geometry (case D1), the agreement between experiment (buckling load) and present theory (critical load) is excellent. The theoretical prediction of Ref. 12 is also very good. For the other two geometries (cases D2 and D3), the agreement seems to be reasonably good (acceptable). For the same reason, the theoretical prediction of Ref. 12 may also be called reasonably good.

Conclusions

The primary observations and conclusions of this study are as follows:

1) When information on the imperfection (shape and amplitude) was available, the experimental verification of the theoretical predictions was very successful. The results of Fig. 1 (group B) and Table 3 (group D) support this contention.

2) A quantitative comparison between the experimental results and theoretical predictions is very difficult to accomplish when there is no information on the shape and amplitude of imperfection. In spite of this, the comparative results for groups A and C are such that they increase the confidence factor in the theoretical predictions.

On the basis of these observations, one may conclude that the solution methodology employed herein yields accurate limit point loads for imperfect, stiffened, laminated, circular cylindrical, thin shells when acted upon by destabilizing loads. Needless to say, in addition to thinness, one must assume that the length-to-radius ratio is not very large (≤ 5), so that the Donnell-type of theory is applicable.

References

[1]Tennyson, R. C., "Buckling of Laminated Composite Cylinders: A Review," *Composites*, Vol. 1, 1975, pp. 17-24.

[2]Sheinman, I., Shaw, D., and Simitses, G. J., "Nonlinear Analysis of Axially-Loaded, Laminated, Cylindrical Shells," *Computers and Structures*, Vol. 16, No. 1, 1983, pp. 131-137. Also *Advances and Trends in Structural and Solid Mechanics*, edited by A. K. Noor and J. M. Housner, Pergamon Press, New York, 1982, pp. 131-137.

[3]Jones, R. M., *Mechanics of Composites Materials*, McGraw-Hill Book Co., New York, 1975.

[4]Sheinman, I. and Simitses, G. J., "Buckling Analysis of Geometrically Imperfect Stiffened Cylinders under Axial Compression," *AIAA Journal*, Vol. 15, March 1977, pp. 374-379.

[5]Hoff, N. J., "The Perplexing Behavior of Thin Circular Cylindrical Shells in Axial Compression," *Israel Journal of Technology*, Vol. 4, No. 1, 1966, pp. 1-21.

[6]Thurston, G. A., "Newton's Method Applied to Problems of Nonlinear Mechanics," *Journal of Applied Mechanics*, Vol. 32, No. 2, 1965, pp. 383-388.

[7]Tene, Y., Epstein, M., and Sheinman, I., "A Generalization of Potter's Method," *Computers and Structures*, Vol. 4, 1974, pp. 1099-1103.

[8]Sheinman, I. and Simitses, G. J., "A Modification of Potter's Method for Diagonal Matrices with Common Unknown," *Computers and Structures*, Vol. 18, No. 2, 1984, pp. 273-275.

[9]Kobayashi, S., Koyama, K., and Seko, H., "Compressive Buckling of Graphite-Epoxy Composite Circular Cylindrical Shells," (abstract and supplement of abstract), Paper presented at AIAA/ASME/ASCE/AHS Structures, Structural Dynamics, and Materials Conference, New Orleans, May 1982; also private communications.

[10]Booton, N., "Buckling of Imperfect Anisotropic Cylinders Under Combined Loading," University of Toronto, Canada, UTIAS Rept. 203, Aug. 1976 (also *Proceedings of AIAA/ASME/ASCE/AHS Structures, Structural Dynamics and Materials Conference*, Bethesda, Md., 1978, pp. 351-358.

[11]Wilkins, D. J. and Love, T. S., "Compression-Torsion Buckling Test of Laminated Composite Cylindrical Shells," AIAA Paper 74-379, 1974.

[12]Tennyson, R. C. and Muggeridge, D. B., "Buckling of Laminated Anisotropic Imperfect Circular Cylinders under Axial Compression," *Journal of Spacecraft and Rockets*, Vol. 10, Feb. 1973, pp. 143-148.

[13]Shaw, D. and Simitses, G. J., "Instability of Laminated Cylinders in Torsion," *Journal of Applied Mechanics*, Vol. 51, No. 1, 1984, pp. 188-191.